

## Research Article

# Synthesis of Carbon-Encapsulated Magnetic Iron Oxide Nanocomposites for Bioapplication

Wubshet Mekonnen Girma 

*Department of Chemistry, Wollo University, Dessie, Ethiopia*

Correspondence should be addressed to Wubshet Mekonnen Girma; [danyfree2004@gmail.com](mailto:danyfree2004@gmail.com)

Received 7 July 2022; Revised 1 September 2022; Accepted 6 September 2022; Published 20 September 2022

Academic Editor: Sameh Ali

Copyright © 2022 Wubshet Mekonnen Girma. This is an open access article distributed under the Creative Commons Attribution License, which permits unrestricted use, distribution, and reproduction in any medium, provided the original work is properly cited.

Carbon-encapsulated  $\text{Fe}_3\text{O}_4$  nanoparticles (NPs) were successfully synthesized from a single precursor using one-step solvothermal methods. X-ray diffraction and transmission electron microscopy were used to characterize the as-prepared NPs, and UV-visible absorbance spectroscopy was used to check their optical properties. The morphological results revealed that  $\text{Fe}_3\text{O}_4$ @C, quasi-spherical  $\text{Fe}_3\text{O}_4$  particles encapsulated by carbon. In addition, the carbon-encapsulated  $\text{Fe}_3\text{O}_4$  NPs were conjugated with folic acid (FA) to be used as biomarkers in the diagnosis and treatment of tumour cells. Fourier transform infrared spectroscopy and UV-visible spectroscopic techniques were used to confirm the conjugation process.

## 1. Introduction

Nanoparticles (NPs) that combine both magnetic and optical properties have attracted attention owing to their wide range of biomedical applications. Magnetic NPs can be tailored as a contrast agent in magnetic resonance imaging (MRI), for separation, detection, targeting, hyperthermia, and photothermal therapy. Magnetic nanocrystalline materials have the disadvantage of rapid degradation/aggregation in the physiological environments of the tumour as well as aqueous solubility due to very high surface area to volume ratio and higher reactivity. This tends to restrict their potential application and investigation of their properties [1]. To overcome this problem encapsulation has been done by different scholars to protect aggregations and exploit their properties to apply for different applications [2, 3]. A number of magnetic NP formulations are currently being developed to meet specific needs; however, little effort has been made to develop a universal combined formulation [4] for cancer applications. As a result, developing a multifunctional magnetic NP formulation that does not compromise fundamental properties is highly desirable. Such formulations have recently been developed to gain various biological functions [5]. These formulations can be used for

not only drug delivery but also MRI visible targeting [6], magnetically targeted photodynamic therapy [7], targeted thermosensitive chemotherapy [8], and luminescence/near-IR/multi-modal imaging [9].

Among different magnetic materials,  $\text{Fe}_3\text{O}_4$  is widely studied magnetic nanocluster and applicable for hyperthermia, MRI, cancer staining, hydrogen storage and supercapacitors, soil remediation, and water treatments. However,  $\text{Fe}_3\text{O}_4$  suffer from two major issues such as rapid agglomeration, oxidation into the physiological environment of the tumours due to large surface area, chemical reactivity, and high surface energy, thus resulting in a loss of magnetism [10, 11]. Therefore, encapsulation/surface modification plays a crucial role in its structure since it can protect the magnetic core from oxidation, thermal and temporary degradation [12]. However,  $\text{Fe}_3\text{O}_4$  coated by polymers, nanogels, micelles, and microcapsules exhibited reduction of magnetic property, increments of particle size, and lower efficiency during drug loading. In addition, it affects the solubility, leads to aggregation, and further affects biocompatibility in living cells in some of these complexes. Therefore, the carbon encapsulation adds additional features to the magnetic NPs such as easy functionalization, electrical properties, as well as catalytic activities. It also helps to

stabilize at physiological and high temperature environment to make it biocompatible in medical applications. Most recent studies showed that folic acid (FA) modified  $\text{Fe}_3\text{O}_4$  NPs are applied for cervical cancer diagnosis [13]. Since recent studies displayed that specific biomarkers on the surface of NPs lead to efficient diagnosis and treatments of cancer [14–16].

In this work, we report a single and rapid synthesis protocol by using the hydrothermal approach from a single precursor, carbon-encapsulated  $\text{Fe}_3\text{O}_4$  NPs are formed via oxidation of  $\text{Fe}^{2+}$  using  $\text{H}_2\text{O}_2$ , by decomposition of ferrocene. The obtained NPs have good magnetic properties with carbon encapsulation, allowing us to conjugate with folic acid and use them in biomedical applications such as diagnosis, therapeutic, environmental remediation, catalysis, energy storage materials, and magnetic devices. The advantages of our formulation are good magnetic properties, good stability, and easy functionalization due to carbon encapsulation. Furthermore, the biocompatibility of the synthesized magnetic material has displayed a minimal toxicity. Therefore, it could have promising applications in biomedical fields.

## 2. Materials and Methods

**2.1. Chemicals.** Ferrocene ( $\text{Fe}(\text{C}_5\text{H}_5)_2$ ,  $\geq 98\%$ ), hydrogen peroxide ( $\text{H}_2\text{O}_2$ , 30%), acetone ( $\text{C}_3\text{H}_6\text{O}$ ,  $\geq 99\%$ ), and 3-(4, 5-dimethylthiazol-2-yl)-2, 5-diphenyltetrazolium bromide (MTT, 97.5%) were obtained from Sigma-Aldrich. Folic acid ( $>98\%$ ) was obtained from TCI. N-hydroxy sulfo succinimide sodium salt (Sulfo-NHS, 97%), ethyl (dimethyl aminopropyl) carbodiimide (EDC, 99%), and N-hydroxysulfo succinimide sodium salt (sulfo-NHS, 97%) were obtained from Alfa-Aesar.

**2.2. Synthesis of  $\text{Fe}_3\text{O}_4$ @C Core/Shell NPs.** The synthesis protocol was done with small modifications from the literature [10]. 0.2 g of ferrocene was dissolved in 60 mL of acetone and subjected to sonication for half an hour. 30% of  $\text{H}_2\text{O}_2$  was slowly added to the solution with continuous stirring for half hour. Afterward, the solution was transferred to Teflon-lined stainless autoclave and allowed to proceed for 16 h at  $180^\circ\text{C}$ . Then, the autoclave was allowed to cool at room temperature. The product was collected after intense sonication by using magnet and washed with acetone to remove unreacted ferrocene. Finally, the obtained  $\text{Fe}_3\text{O}_4$ @C NPs were dried at  $40^\circ\text{C}$  in vacuum.

**2.3. Conjugation of  $\text{Fe}_3\text{O}_4$ @C with Folic Acid.** To activate the carboxylic group of  $\text{Fe}_3\text{O}_4$ @C NPs, EDC (10 mg) and sulfo-NHS (10 mg) in 1 mL of MES buffer were added to 2 mL of  $\text{Fe}_3\text{O}_4$ @C NPs solution (20 mg/mL) and then stirred in the dark at room temperature for 30 min. Subsequently, 1 mL of MES solution containing folic acid ( $2.26 \times 10^{-3}$  mmol) was added to the activated  $\text{Fe}_3\text{O}_4$ @C NPs solution, and the mixture was stirred gently at room temperature in the dark. After 16 h, a magnet was used to separate the final product ( $\text{Fe}_3\text{O}_4$ @C-FA).

**2.4. Cell Culture and Cell Viability Test.** Human cervical cancer cells (HeLa) were cultivated in Dulbecco's modified eagle's medium (DMEM, Hyclone), added with 1% non-essential amino acids, 1% sodium pyruvate, 1% L-glutamine, 1% antibiotic antimycotic formulation, and 10% fetal bovine serum at  $37^\circ\text{C}$ , in a humidified 5%  $\text{CO}_2$  atmosphere.

$\text{Fe}_3\text{O}_4$ @C-FA *in vitro* cytotoxicity was assessed using the MTT assay. Cells ( $\sim 5 \times 10^4$ /well) were cultured in a 24-well plate for 24 h. Afterward, the medium was washed three times and changed with 200  $\mu\text{L}$  fresh culture medium contain various concentrations (0, 25, 50, 100, 200, 500, and 1000  $\mu\text{g}/\text{mL}$ ) of  $\text{Fe}_3\text{O}_4$ @C-FA and cultured for additional 24 h. Then, the cultured cells washed with PBS three times and replaced with fresh medium followed by adding 1 mL of MTT aqueous solution (500  $\mu\text{g}/\text{mL}$ ) was added to each well, and the cells were incubated at  $37^\circ\text{C}$  in a 5%  $\text{CO}_2$  humidified incubator for another 4 h. Subsequently, the medium was removed, and cells were dispersed into 1 mL of dimethyl sulfoxide/well and incubated for 15 min. Finally, the optical density of the cell suspension was measured at 570 nm using a Biotek Powerwave XS plate reader. The experiment was done three times under the same conditions. The cell viability was estimated with the following equation:

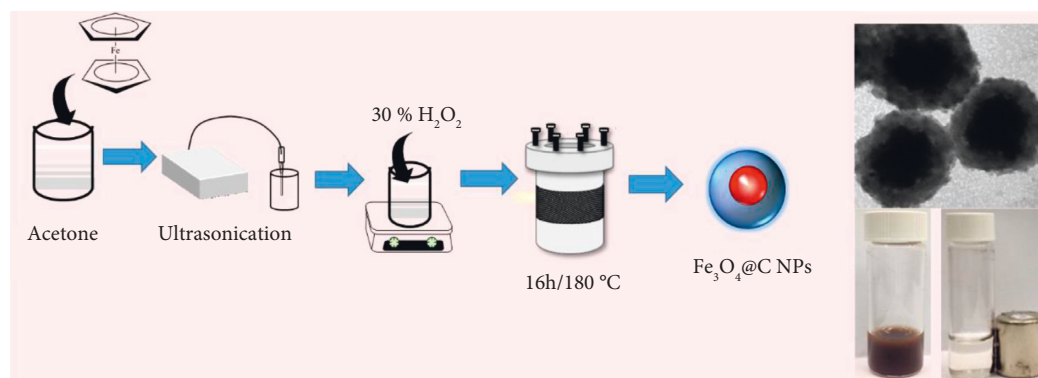
$$\text{cell viability (\%)} = \frac{\text{optical density of treated sample}}{\text{optical density of control sample}} \times 100\%. \quad (1)$$

**2.5. Characterization.** The morphology was characterized using transmission electron microscopy (TEM) and FEI Tecnai G2 F20 microscope (Philips, Amsterdam, Holland) with an accelerating voltage of 200 kV. X-ray diffraction (XRD) patterns were obtained using a Bruker D8 Discover X-ray diffractometer. UV-visible absorbance spectra were acquired on Jasco V-630 spectrophotometers. Fourier transform infrared (FT-IR) spectra were obtained by Nicolet 5700 FT-IR spectrometer.

## 3. Results and Discussion

**3.1. Synthesis and Characterizations of  $\text{Fe}_3\text{O}_4$ @C.** As shown in Scheme 1, Ferrocene has been employed as an adaptable precursor to synthesize carbon-encapsulated  $\text{Fe}_3\text{O}_4$  NPs since it can offer both iron and carbon sources [17, 18]. Acetone were used as a synthesis solvent and ultrasonication were used to homogenise ferrocene. Hydrogen peroxide were added to oxidize ferrocene into  $\text{Fe}_3\text{O}_4$ @C. Precursor thermally decompose and monomers accumulate in the solution during the heat treatment. Burst nucleation occurred when the monomer concentration exceeded a critical level for nucleation, followed by the growth of  $\text{Fe}_3\text{O}_4$ @C NPs.

Powder X-ray diffraction technique was applied to identify the crystalline structure of the as-prepared  $\text{Fe}_3\text{O}_4$ @C NPs. Figure 1 clearly displays five diffraction peaks that match with (220), (311), (222), (400), (511), and (440) lattice planes of  $\text{Fe}_3\text{O}_4$  (JCPDS 19-0629). The higher diffraction intensity implies that higher crystalline magnetic



SCHEME 1: The schematic representations of one-step fabrications of  $\text{Fe}_3\text{O}_4@\text{C}$  from a single precursor.

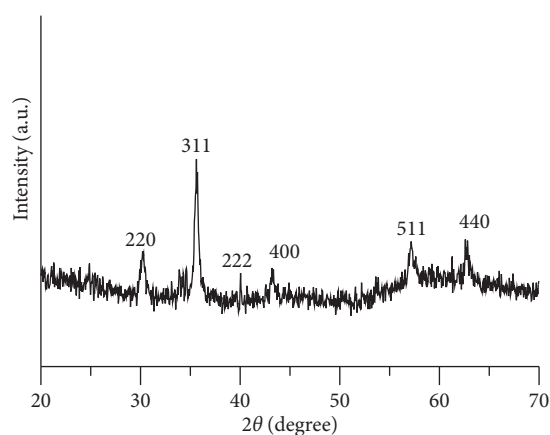


FIGURE 1: The XRD patterns of as-prepared  $\text{Fe}_3\text{O}_4@\text{C}$ .

$\text{Fe}_3\text{O}_4$  particles synthesized by the solvothermal method. It should be noted that due to the thin layer of the carbon shell on  $\text{Fe}_3\text{O}_4$  nanospheres, no peaks for amorphous carbon were observed, suggesting the structure of carbon is amorphous in the sample. There were no other impurity peaks detected, indicating the high purity of the synthesized products.

Figure 2 displays the typical TEM images of the as-synthesized  $\text{Fe}_3\text{O}_4@\text{C}$  NPs to see the morphology and microstructures. At first glance, it is clear from Figures 2(a) and 2(b) that the products have a sphere-shaped morphology. It should be noted that the majority of  $\text{Fe}_3\text{O}_4$  particles were coated in carbon close scrutiny (Figures 2(c) and 2(d)) demonstrates that the thickness of the carbon layer on the surface of  $\text{Fe}_3\text{O}_4$  was very thin and uneven. The dimensions of the  $\text{Fe}_3\text{O}_4$  core were significantly larger than the carbon shell layer. Generally, well-dispersed NPs with  $\text{Fe}_3\text{O}_4$  encapsulated by carbon matrix from a single precursor. Furthermore, agglomeration of NPs was not seen, this might be due to successful encapsulation of the NPs.

The optical properties of the as-prepared NPs were studied using absorbance spectroscopy. Both  $\text{Fe}_3\text{O}_4@\text{C}$  and  $\text{Fe}_3\text{O}_4@\text{C-FA}$  showed absorbance profile in UV and visible spectral ranges 200–1000 nm with long tail in longer wave length as shown in Figure 3. The absorption profiles of

$\text{Fe}_3\text{O}_4@\text{C-FA}$  showed similar profile as its original NPs except intensity change.

As depicted in Figure 4, FT-IR spectra were chosen to identify the functional groups in each conjugation steps. A broad peak appearing above  $3300\text{ cm}^{-1}$  were assigned to the stretching vibrations of -OH and - $\text{NH}_2$  groups. The stretching peaks appearing around  $2953\text{ cm}^{-1}$  were assigned to C-H in both  $\text{Fe}_3\text{O}_4@\text{C}$  and  $\text{Fe}_3\text{O}_4@\text{C-FA}$ . The stretching peaks appearing around  $2343\text{ cm}^{-1}$  were due to C=O=C searching frequencies. The stretching peaks appearing around  $1530\text{--}1680\text{ cm}^{-1}$  were assigned to C=C searching frequencies. After conjugation, thus C=C peaks showed shift. A medium band appearing around  $1424\text{ cm}^{-1}$  in  $\text{Fe}_3\text{O}_4@\text{C}$  NPs was assigned C-H bending vibrations. This peak in  $\text{Fe}_3\text{O}_4@\text{C-FA}$  shifted to  $1410\text{ cm}^{-1}$  with intensity decrement which revealed successful conjugations.

The *in vitro* cytotoxicity of the  $\text{Fe}_3\text{O}_4@\text{C-FA}$  was investigated by the MTT assay against HeLa cells. As displayed in Figure 5, the viability of cells was greater than 95% after treatments of cells for 48 h at different concentrations of  $\text{Fe}_3\text{O}_4@\text{C-FA}$  (0, 25, 50, 100, 200, 500, and  $1000\text{ }\mu\text{g/mL}$ ). Accordingly,  $\text{Fe}_3\text{O}_4@\text{C-FA}$  showed lower cytotoxicity, which makes it competent for future clinical applications. Thus, the results confirmed that  $\text{Fe}_3\text{O}_4@\text{C-FA}$  was highly biocompatible with low toxicity to serve as bioapplications.

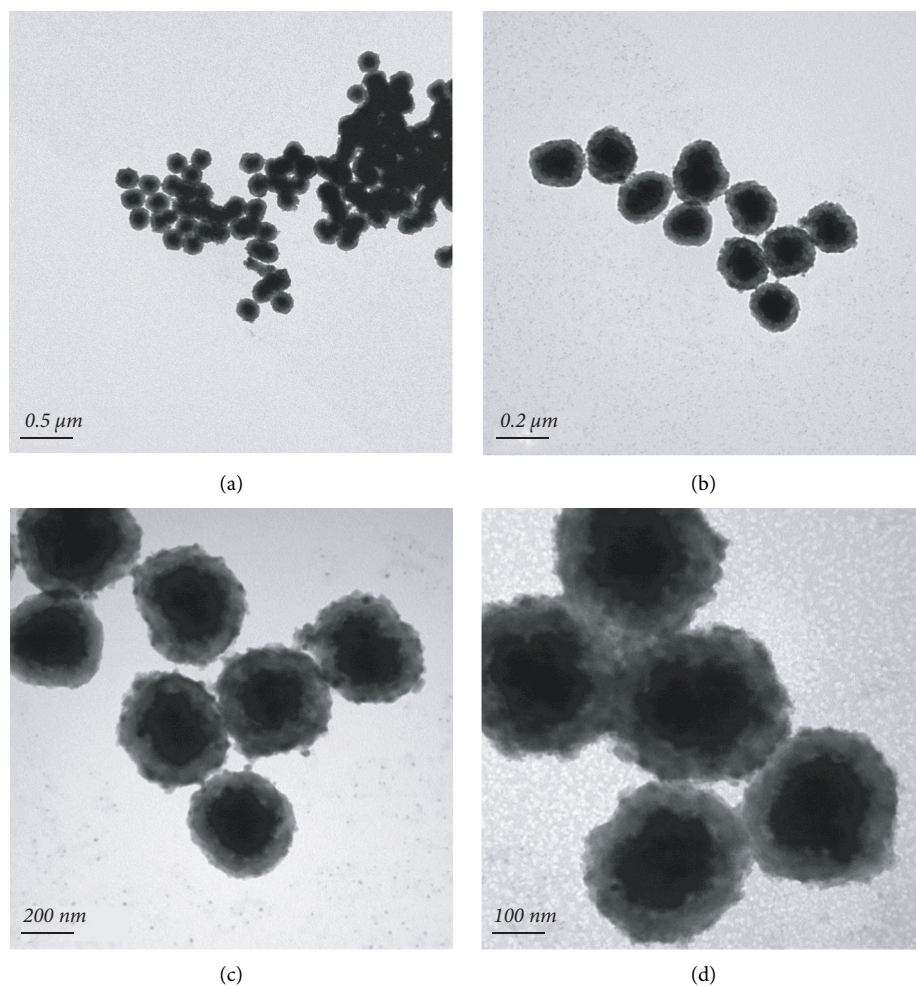


FIGURE 2: (a–d) The TEM images of the as-prepared  $\text{Fe}_3\text{O}_4$  NPs at different scale bars.

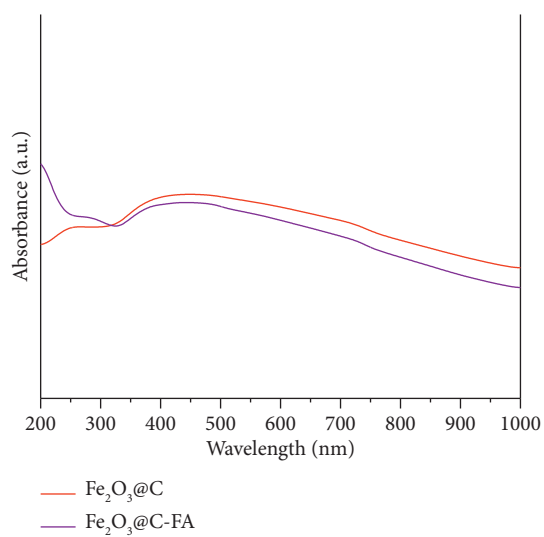


FIGURE 3: The absorbance spectra of  $\text{Fe}_3\text{O}_4/\text{C}$  and  $\text{Fe}_3\text{O}_4/\text{C-FA}$ .

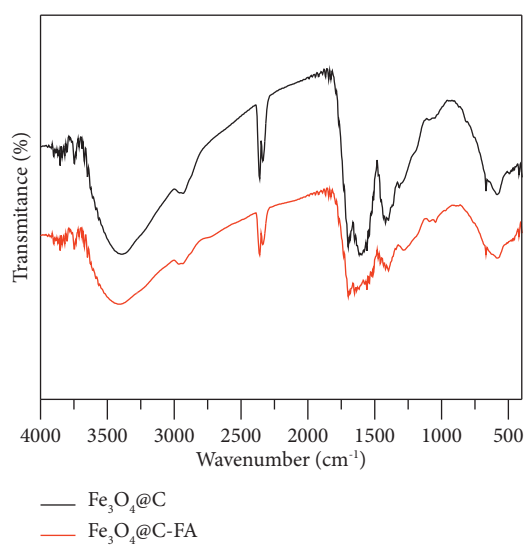


FIGURE 4: The FT-IR spectra of  $\text{Fe}_3\text{O}_4/\text{C}$  and  $\text{Fe}_3\text{O}_4/\text{C-FA}$ .

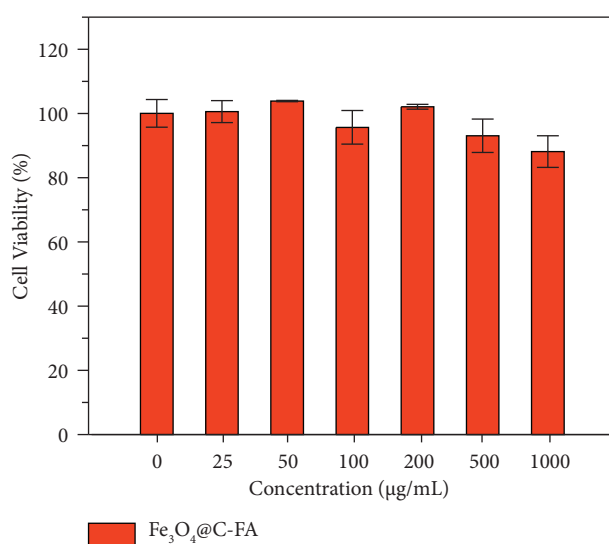


FIGURE 5: The MTT assay of HeLa cells cell viable after incubations of different concentrations (0, 25, 50, 100, 200, 500, and 1000 µg/mL) of  $\text{Fe}_3\text{O}_4\text{@C-FA}$  at 37°C for 48 h. Error bars indicate the mean  $\pm$  standard deviations ( $n = 3$ ).

#### 4. Conclusions

In conclusion, a simple one-pot solvothermal synthesis method using a single precursor was developed to serve as a biomedical probe in the diagnosis and therapy. The entire synthesis protocol for carbon-encapsulated iron oxide leads to magnetic, stable, and biocompatible NPs and is fast, reproducible, and scalable. The TEM microstructures revealed that the  $\text{Fe}_3\text{O}_4$  NPs are carbon encapsulated, and thus free of aggregation, which is a common problem in most magnetic nanoparticles. The cytotoxicity study confirmed the low toxicity for biological applications.

#### Data Availability

All data are included within the article.

#### Conflicts of Interest

The author declares that there are no conflicts of interest.

#### References

- [1] X. Sun, A. Gutierrez, M. J. Yacaman, X. Dong, and S. Jin, "Investigations on magnetic properties and structure for carbon encapsulated nanoparticles of Fe, Co, Ni," *Materials Science and Engineering*, vol. 286, no. 1, pp. 157–160, 2000.
- [2] H. Wang, Y. B. Sun, Q. W. Chen, Y. F. Yu, and K. Cheng, "Synthesis of carbon-encapsulated superparamagnetic colloidal nanoparticles with magnetic-responsive photonic crystal property," *Dalton Transactions*, vol. 39, no. 40, pp. 9565–9569, 2010.
- [3] H. Wang, Q. W. Chen, Y. F. Yu, K. Cheng, and Y. B. Sun, "Size- and solvent-dependent magnetically responsive optical diffraction of carbon-encapsulated superparamagnetic colloidal photonic crystals," *Journal of Physical Chemistry C*, vol. 115, no. 23, pp. 11427–11434, 2011.
- [4] K. Montet-Abou, X. Montet, R. Weissleder, and L. Josephson, "Cell internalization of magnetic nanoparticles using transfection agents," *Molecular Imaging*, vol. 6, no. 1, p. 7290, Article ID 00028, 2007.
- [5] J. R. McCarthy and R. Weissleder, "Multifunctional magnetic nanoparticles for targeted imaging and therapy," *Advanced Drug Delivery Reviews*, vol. 60, no. 11, pp. 1241–1251, 2008.
- [6] J. S. Guthi, S. G. Yang, G. Huang et al., "MRI-visible micellar nanomedicine for targeted drug delivery to lung cancer cells," *Molecular Pharmaceutics*, vol. 7, no. 1, pp. 32–40, 2010.
- [7] L. O. Cinteza, T. Y. Ohulchanskyy, Y. Sahoo, E. J. Bergey, R. K. Pandey, and P. N. Prasad, "Diacyllipid micelle-based nanocarrier for magnetically guided delivery of drugs in photodynamic therapy," *Molecular Pharmaceutics*, vol. 3, no. 4, pp. 415–423, 2006.
- [8] P. Pradhan, J. Giri, F. Rieken et al., "Targeted temperature sensitive magnetic liposomes for thermo-chemotherapy," *Journal of Controlled Release*, vol. 142, no. 1, pp. 108–121, 2010.
- [9] R. Guo, L. Zhang, H. Qian, R. Li, X. Jiang, and B. Liu, "Multifunctional nanocarriers for cell imaging, drug delivery, and near-IR photothermal therapy," *Langmuir*, vol. 26, no. 8, pp. 5428–5434, 2010.
- [10] W. Xie, L. Gu, X. Sun et al., "Ferrocene derived core-shell structural  $\text{Fe}_3\text{O}_4\text{@C}$  nanospheres for superior lithium storage properties," *Electrochimica Acta*, vol. 220, pp. 107–113, 2016.
- [11] A. Mohammadi, M. Barikani, and M. Barmar, "Effect of surface modification of  $\text{Fe}_3\text{O}_4$  nanoparticles on thermal and mechanical properties of magnetic polyurethane elastomer nanocomposites," *Journal of Materials Science*, vol. 48, no. 21, pp. 7493–7502, 2013.
- [12] Y. Li and W. Duan, "Highly significant fluorescence enhancement effect of silver-deposited  $\text{Fe}_3\text{O}_4\text{@C}$  core/shell nanoparticles for detection of dyes and fluorescein," *Composites Communications*, vol. 28, Article ID 100964, 2021.
- [13] M. Ramezani Farani, M. Azarian, H. Heydari Sheikh Hossein et al., "Folic acid-adorned curcumin-loaded iron oxide nanoparticles for cervical cancer," *ACS Applied Bio Materials*, vol. 5, no. 3, pp. 1305–1318, 2022.
- [14] N. Rabiee, M. Bagherzadeh, A. M. Ghadiri et al., "Bio-multifunctional noncovalent porphyrin functionalized carbon-based nanocomposite," *Scientific Reports*, vol. 11, no. 1, pp. 6604–6615, 2021.
- [15] N. Rabiee, M. T. Yarak, S. M. Garakani et al., "Recent advances in porphyrin-based nanocomposites for effective targeted imaging and therapy," *Biomaterials*, vol. 232, Article ID 119707, 2020.
- [16] A. Bakhshian Nik, H. Zare, S. Razavi et al., "Smart drug delivery: capping strategies for mesoporous silica nanoparticles," *Microporous and Mesoporous Materials*, vol. 299, Article ID 110115, 2020.
- [17] Y. Lu, Z. Zhu, and Z. Liu, "Carbon-encapsulated Fe nanoparticles from detonation-induced pyrolysis of ferrocene," *Carbon*, vol. 43, no. 2, pp. 369–374, 2005.
- [18] H. Hou, A. K. Schaper, F. Weller, and A. Greiner, "Carbon nanotubes and spheres produced by modified ferrocene pyrolysis," *Chemistry of Materials*, vol. 14, no. 9, pp. 3990–3994, 2002.